Chemical Science

ROYAL SOCIETY OF CHEMISTRY

EDGE ARTICLE

View Article Online
View Journal | View Issue

Check for updates

Cite this: *Chem. Sci.*, 2025, **16**, 17487

All publication charges for this article have been paid for by the Royal Society of Chemistry

Ultrastrong circularly polarized electroluminescence achieved by chiral co-assembly of a liquid crystal-functionalized carbazole derivative

Hang Li,[a] Dong Li,[a] Zhenhao Jiang,[a] Yuxiang Wang *[b] and Yixiang Cheng *[a]

Received 12th July 2025
Accepted 25th August 2025

DOI: 10.1039/d5sc05196g

rsc.li/chemical-science

Circularly polarized organic light-emitting diodes (CP-OLEDs) exhibiting circularly polarized electroluminescence (CP-EL) properties hold significant promise for future display technologies. However, enhancing the electroluminescence dissymmetry factor (g_{EL}) remains a substantial challenge. Herein, ultrastrong CP-EL emissions are achieved using a liquid crystal (LC)-functionalization strategy under the regulation of chiral co-assembly. The LC molecule **3CzPCH** containing carbazole and mesogenic units could be readily synthesized using Suzuki coupling reactions. When doping chiral inducers ***R*/*S*-D** into **3CzPCH**, the chiral co-assemblies formed helical nanofibers upon 120 °C annealing treatment and emitted strong deep-blue circularly polarized luminescence (CPL) with $|g_{lum}|$ of 0.13 (λ_{em} = 422 nm, Φ_{FL} = 34%). Most importantly, these chiral co-assemblies served as the emitting layers (EMLs) of CP-OLEDs, reaching an ultrastrong deep-blue CP-EL with a $|g_{EL}|$ value up to 0.47 (λ_{EL} = 440 nm). The corresponding *Q*-factor (EQE × $|g_{EL}|$) of 1.12 × 10^{-2} represents one of the highest values reported for CP-OLEDs. This study demonstrates that the LC-functionalization strategy effectively enables intense CP-EL, paving the way for high-performance CP-OLEDs.

Introduction

Circularly polarized organic light-emitting diodes (CP-OLEDs) have attracted significant attention due to their potential applications in next-generation display technologies.[1–4] Compared to non-polarized OLEDs, CP-OLEDs emit circularly polarized light directly, avoiding complex device architectures and energy loss.[5,6] To date, various types of emitting layer (EML) materials for CP-OLEDs have been reported, including chiral small molecules, polymers, thermally activated delayed fluorescence (TADF) materials, and metal complexes.[7–14] While these devices often exhibit high electroluminescence (EL) performance, most of them suffer from low electroluminescence dissymmetry factors (g_{EL}), limiting their practical applications. Therefore, enhancing the g_{EL} values remains critically important for advancing CP-OLED development. In recent years, chiral supramolecular co-assembly has been considered as an efficient strategy to obtain high g_{lum} values in circularly polarized luminescence (CPL) materials.[15,16] Through non-covalent interactions like π–π stacking, electrostatic interactions and intermolecular hydrogen bonding, chiral co-assemblies form highly ordered helical structures that significantly enhance CPL signals.[17–19] This approach has also proven effective for developing the EML materials of CP-OLEDs.[20] Since Fuchter *et al.* utilized co-assembled EMLs of achiral emissive polymer F8BT and chiral aza[6]helicene to realize a high g_{EL} value of 0.2,[21] numerous CP-OLEDs exhibiting high CP-EL performance have been realized through the supramolecular co-assembly of F8BT or other fluorene-based polymers doped with chiral inducers.[22–27] For example, Chen *et al.* achieved a narrowband CP-EL with a g_{EL} value of 0.16 by using ternary co-assemblies of F8BT, chiral inducers, and an achiral TADF emitter.[25] Our group designed a series of polyfluorenes to construct chiral co-assemblies between polymers for CP-OLEDs, achieving a maximum g_{EL} value of 0.014.[27]

In order to achieve macroscopic uniformly chiral co-assembly, liquid crystal (LC) materials are promising candidates.[28–30] Among them, chiral nematic LCs with periodic helical superstructures can significantly promote the amplification of CPL emissions.[31–35] However, conventional LC molecules are typically electrical insulators with poor thermal stability, rendering them unsuitable for EMLs of CP-OLEDs. Fluorene derivatives combining inherent LC properties and carrier mobilities are used as the EMLs of CP-OLEDs, which can achieve high g_{EL} values especially by the twisted stacking structures in EMLs.[36–41] Nevertheless, such high g_{EL} values often

[a]*State Key Laboratory of Analytical Chemistry for Life Science, School of Chemistry and Chemical Engineering, Nanjing University, Nanjing 210023, China. E-mail: yxcheng@nju.edu.cn*

[b]*Jiangsu Key Laboratory of Advanced Catalytic Materials and Technology, School of Petrochemical Engineering, Changzhou University, Changzhou, Jiangsu 213164, China. E-mail: wangyx@cczu.edu.cn*

Open Access Article. Published on 25 August 2025. Downloaded on 6/15/2026 6:01:51 AM. This article is licensed under a Creative Commons Attribution-NonCommercial 3.0 Unported Licence.

Open Access Article. Published on 25 August 2025. Downloaded on 6/15/2026 6:01:51 AM. This article is licensed under a Creative Commons Attribution-NonCommercial 3.0 Unported Licence.

depend on excessively thick EMLs, leading to compromised luminance and efficiency. To design conductive LCs towards efficient CP-EL, the "LC-functionalization" strategy is an alternative approach. By connecting π-conjugated moieties with mesogenic units, conductive LCs can be designed for use in optoelectronic devices. Although this strategy has been employed to construct versatile supramolecularly assembled materials,[42–44] it is rarely applied to chiral co-assembled EML materials for improving CP-EL performance. In 2020, Wang *et al.* reported a chiral platinum complex LC designed *via* this strategy by incorporating mesogenic units into its ligands, which was employed as a doped EML within a host matrix to achieve a $|g_{EL}|$ value of 0.06 after annealing.[45] However, this doped approach risks disrupting the desired mesophase, thereby compromising CP-EL performance.[46–48] Recently, our group reported non-doped CP-OLEDs with a $|g_{EL}|$ of 0.019 using chiral co-assemblies of LC-functionalized polyacrylates as the EMLs.[49] Nevertheless, these modest $|g_{EL}|$ values still leave room for improvement in developing high-performance CP-OLEDs.

Herein, we design a conductive carbazole derivative **3CzPh**, which does not exhibit LC properties. Using the LC-functionalization strategy, the nematic LC molecule **3CzPCH** is readily synthesized by replacing two phenyl groups with mesogenic units (Scheme 1a). Dihedral angle-anchored binaphthalene derivatives with identical mesogenic units (***R*/*S*-D**) were selected as chiral inducers to enable chiral co-assembly formation after annealing treatment (Scheme 1b). **3CzPCH**+***R*/*S*-D** exhibited enhanced CPL signals after thermal annealing, reaching a maximum $|g_{lum}|$ value of 0.13 (λ_{em} = 422 nm, Φ_{FL} = 34%) (Scheme 1c and d). However, **3CzPh**+***R*/*S*-D** displayed negligible chiroptical signals before and after thermal annealing due to the absence of chiral co-assembly. Furthermore, solution-processed non-doped CP-OLEDs employing the chiral co-assembled **3CzPCH**+***R*/*S*-D** as the EMLs demonstrated ultrastrong CP-EL performance, achieving a $|g_{EL}|$ of 0.47 (λ_{EL} = 440 nm) and *Q*-factor (EQE × $|g_{EL}|$) of 1.12×10^{-2} (Scheme 1e). This work demonstrates that intense CP-EL can be achieved by the chiral co-assemblies of the LC-functionalized carbazole derivative, providing an effective strategy for developing high-performance CP-OLEDs.

Results and discussion

Synthesis and characterization

The carbazole unit is selected as the building block due to its remarkable charge carrier mobility and structural tunability.[50,51] A branched alkyl chain was incorporated at a nitrogen atom to improve solubility in organic solvents. The mesogenic unit, (4-pentylcyclohexyl)phenyl, was conjugated on carbazole groups to obtain the LC-functionalized molecule **3CzPCH**. For comparison, **3CzPh** with two phenyl units instead of mesogenic units was also synthesized. Both compounds were readily prepared *via* Suzuki coupling reactions. Detailed synthesis procedures and characterizations are available in the SI. Their thermal properties were evaluated by thermogravimetric analysis (TGA) and differential scanning calorimetry (DSC). TGA results showed that these two compounds had high decomposition temperatures (T_d, 5% weight loss temperature) of 473 °C and 442 °C (Fig. S1a), indicating good thermal stabilities. DSC results indicated that **3CzPCH** had two phase transition temperatures, which could be assigned to a melting point (T_m) of 87.1 °C and an isotropic point (T_i) of 203.1 °C (Fig. S1b). For **3CzPh**, only a T_m of 98.6 °C was observed. The lower T_m of **3CzPCH** results from increased conformational flexibility conferred by its additional alkyl units.

Electrochemical properties

Their electrochemical properties were evaluated by cyclic voltammetry (CV) in degassed dichloromethane. The results are summarized in Fig. S2 and Table S1. Based on the onset voltages of oxidation curves, the highest occupied molecular orbital (HOMO) levels were determined to be −5.21 eV for **3CzPCH** and −5.15 eV for **3CzPh**. And according to their energy gap (E_g) values calculated from the absorption spectra of neat films, the lowest unoccupied molecular orbital (LUMO) levels were

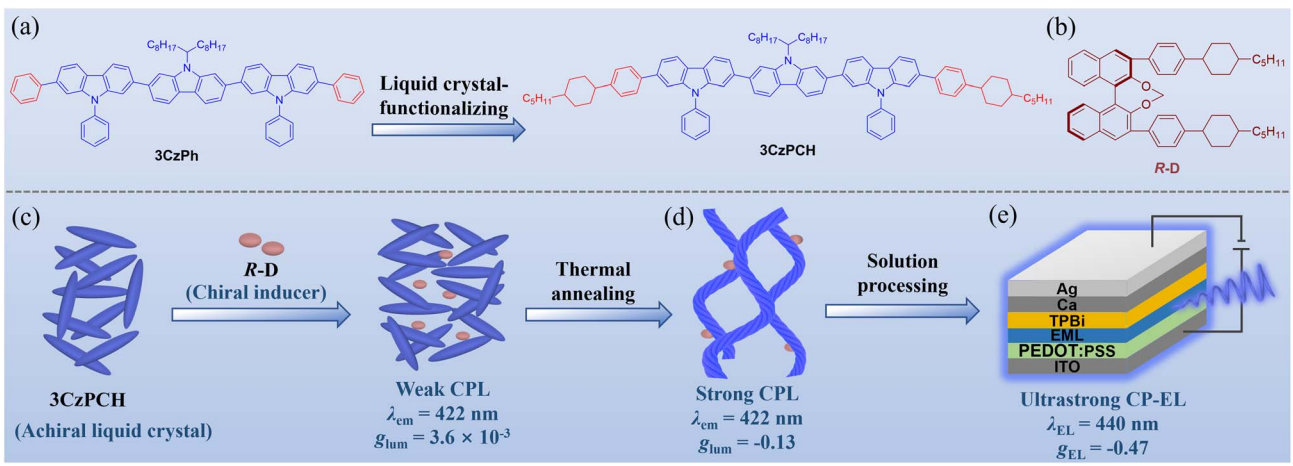

Scheme 1 (a) Chemical structures of **3CzPh** and liquid crystal-functionalized **3CzPCH**; (b) chemical structure of chiral inducer ***R*-D**; schematic diagram of the chiral co-assembly process (c) before and (d) after thermal annealing; (e) the device configuration of CP-OLEDs.

© 2025 The Author(s). Published by the Royal Society of Chemistry

Open Access Article. Published on 25 August 2025. Downloaded on 6/15/2026 6:01:51 AM. This article is licensed under a Creative Commons Attribution-NonCommercial 3.0 Unported Licence.

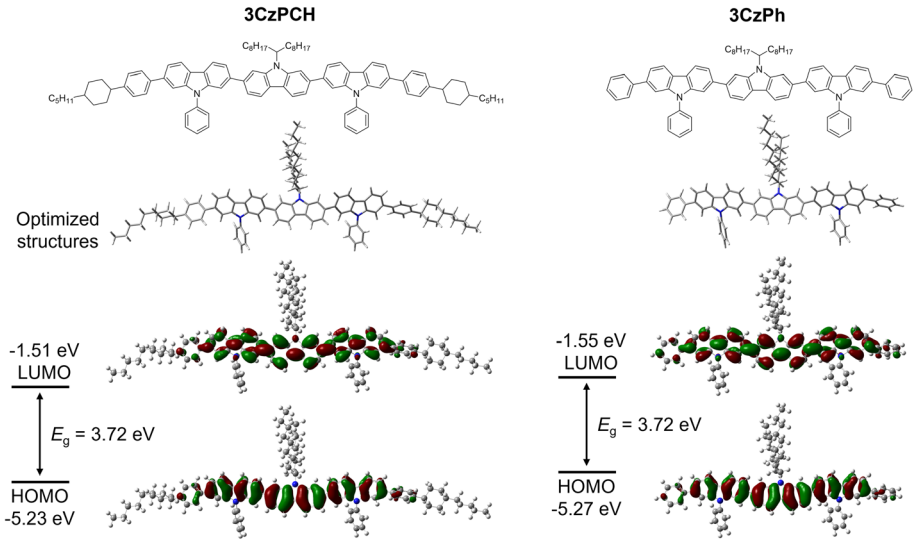

Fig. 1 Optimized structures and HOMO/LUMO distributions of **3CzPCH** and **3CzPh**.

calculated to be −1.94 eV for **3CzPCH** and −1.93 eV for **3CzPh**, respectively. To probe the frontier orbital distributions, density functional theory (DFT) calculations at the B3LYP-D3(BJ)/6-311G* level were performed on these two molecules. The computed HOMO/LUMO energy levels were −5.23/−1.51 eV for **3CzPCH** and −5.27/−1.55 eV for **3CzPh**. As shown in Fig. 1, **3CzPCH** and **3CzPh** have similar HOMO/LUMO spatial distributions and E_g values due to their identical conjugated structures. Furthermore, the HOMO/LUMO orbitals are predominantly located on the three carbazole units, which is conducive to facilitating effective chirality transfer in chiral co-assemblies.

Liquid crystal behaviors

The LC mesophase behaviors of the compounds were characterized by polarized optical microscopy (POM) and small/wide angle X-ray scattering (SAXS/WAXS) investigations. Upon heating from room temperature, the birefringence texture of **3CzPCH** was observed, confirming its LC properties. Its LC phase temperature range was determined to be 87–208 °C, consistent with the DSC results. Upon cooling from isotropic point to 120 °C, a distinct thread-like texture was observed, indicating its nematic LC phase (Fig. 2a). With the doping of chiral inducer ***R*-D**, the textures gradually turned to be indistinguishable (Fig. 2b–f). The SAXS/WAXS profiles further supported the nematic phase assignment, displaying only a broad peak at $q \approx 13.2\ nm^{-1}$ (Fig. S3). In contrast, **3CzPh** showed no birefringence textures during heating or cooling. Combined with its DSC profile lacking mesophase transition peaks, it can be concluded that **3CzPh** exhibits no LC properties. These results suggest that the mesogenic units are crucial for the LC behaviors of carbazole-based derivatives.

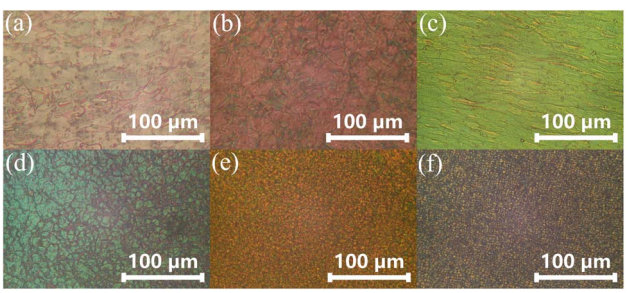

Fig. 2 POM images of **3CzPCH** doped with different wt% amounts of ***R*-D** at 120 °C. (a) 0 wt%; (b) 1 wt%; (c) 3 wt%; (d) 5 wt%; (e) 7 wt%; (f) 10 wt%.

Photophysical properties

The photophysical properties of **3CzPCH** and **3CzPh** were studied by ultraviolet–visible (UV–vis) absorption and photoluminescence (PL) emission spectra. Due to their identical conjugated core structures, both compounds have similar absorption and emission profiles (Table S2). In THF solutions, two characteristic absorption bands are observed at approximately 260 nm and 360 nm (Fig. S4a), which can be assigned to the π–π* transition of single carbazole moieties and extended conjugated structures, respectively. The PL spectra display dual emission peaks at 408 nm and 427 nm, attributed to different vibronic transitions (λ_{0-0} and λ_{0-1}).[52,53] For spin-coated films of **3CzPCH** and **3CzPh**, PL peaks appeared at 422/440 nm and 422/442 nm, which showed a red-shift compared to those in THF solutions (Fig. S4b). The photoluminescence quantum yields (Φ_{FL}) of the thin films were measured to be 34% for **3CzPCH** and 21% for **3CzPh**, respectively. The higher Φ_{FL} of **3CzPCH** could be attributed to the suppression of aggregation-caused quenching by its additional alkyl chains.[54,55]

Chiroptical properties

The chiroptical properties of **3CzPCH** and **3CzPh** doped with chiral inducers were investigated. When doping with varying

Open Access Article. Published on 25 August 2025. Downloaded on 6/15/2026 6:01:51 AM. This article is licensed under a Creative Commons Attribution-NonCommercial 3.0 Unported Licence.

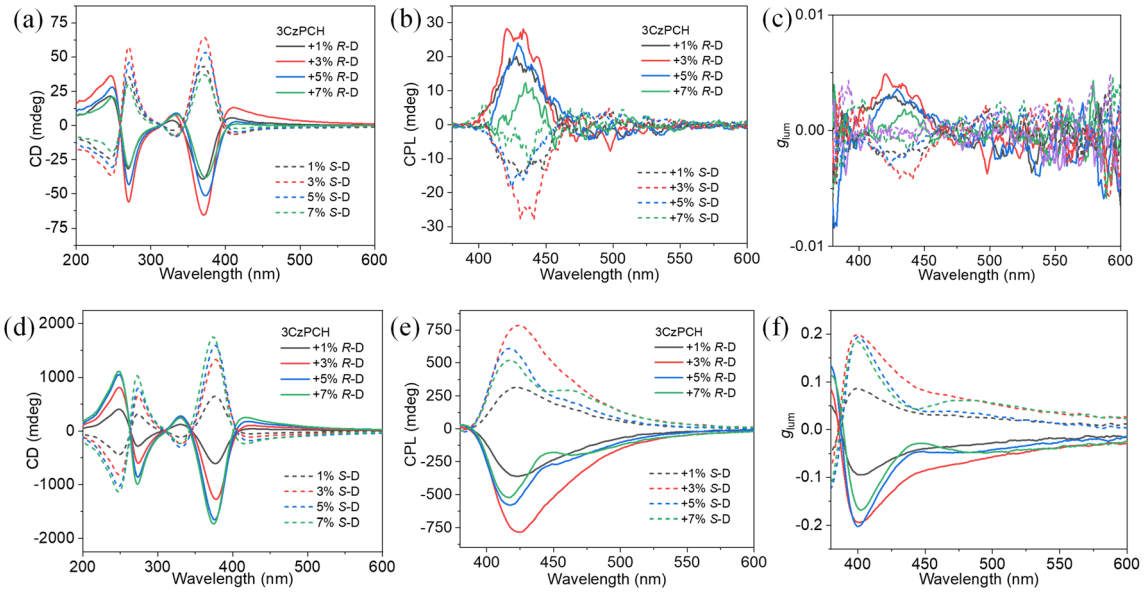

Fig. 3 (a and d) CD spectra, (b and e) CPL spectra, and (c and f) g_{lum} value curves of **3CzPCH** doped with different wt% amounts of ***R*/*S*-D** (a–c: before thermal annealing; d–f: after thermal annealing at 120 °C).

weight percentage of the chiral inducer ***R*/*S*-D**, **3CzPCH+*R*/*S*-D** exhibited a bisignate Cotton effect at 260 nm and a monosignate Cotton effect at 370 nm before thermal annealing (Fig. 3a). Their CPL signals were very weak, with a maximum $|g_{lum}|$ value of 3.6×10^{-3} ($\lambda_{em} = 422$ nm) at 3 wt% doping of ***R*/*S*-D** (Fig. 3b and c). Remarkably, both CD and CPL signals were greatly enhanced after thermal annealing at 120 °C for 20 min (Fig. 3d–f), due to the formation of a chiral co-assembled nematic phase. According to Fig. S5, 120 °C was the optimal annealing temperature. It was observed that the CPL signals were reversed after annealing. Specifically, the annealed films of **3CzPCH** doped with 3 wt% ***R*/*S*-D** displayed the strongest CPL emissions, with $|g_{lum}|$ values reaching up to 0.13. In addition, no significant changes were observed in the CPL signals upon rotating or flipping the films (Fig. S6), thereby ruling out contributions from linear dichroism and linear birefringence to the observed strong CPL signals.[56] In contrast, **3CzPh** doped with chiral inducers displayed only weak CD signals at around 210/270 nm and negligible CPL signals (Fig. S7). These chiroptical signals showed no detectable changes after thermal annealing, indicating the absence of the chiral co-assembly process required for higher-order chiral superstructures. Collectively, these results demonstrate that the mesogenic units are essential for enabling chiral co-assembly and achieving significant amplification of chiroptical signals in carbazole-based derivatives.

Morphology study

Morphologies of chiral co-assemblies **3CzPCH/3CzPh+*R*-D** at different concentrations were characterized by scanning electron microscopy (SEM) to further investigate their chiral co-assembly mechanism. At a high concentration (10 mg mL^{-1}), a smooth surface morphology was observed due to the accumulation of samples (Fig. 4a and d). Upon decreasing the concentration to 10^{-1} mg mL^{-1}, the annealed film of **3CzPCH+*R*-D** exhibited linear stripes compared to the featureless morphology of the unannealed film (Fig. 4b and e). At a lower concentration (10^{-3} mg mL^{-1}), it is obvious that the annealed **3CzPCH+*R*-D** formed orderly left-handed helical nanofibers (Fig. 4f). In contrast, the unannealed **3CzPCH+*R*-D** only showed irregular aggregates interspersed with a limited amount of fibrillar structures, which displayed right-handed helicity (Fig. 4c and S8). Therefore, the reversed CPL signals observed in **3CzPCH+*R*/*S*-D** can be attributed to the helical inversion of nanofibers during thermal annealing. We also studied the morphologies of **3CzPCH** without chiral inducers, which could only form spherical aggregates after thermal annealing (Fig. S9). For **3CzPh** and **3CzPh+*R*-D**, they showed irregular accumulation microstructures before and after thermal annealing, without any chiral co-assembly behaviors (Fig. S10 and S11). The above results indicate that the chiral co-

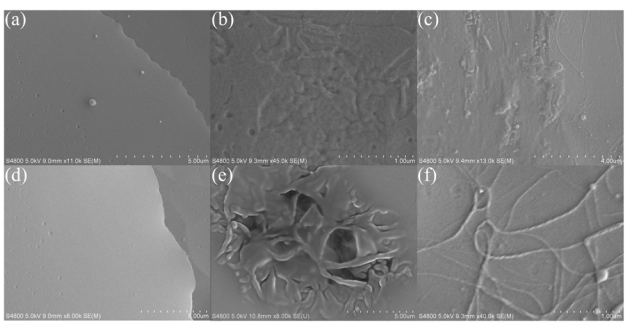

Fig. 4 SEM images of **3CzPCH**+3 wt% ***R*-D** (a–c) before and (d–f) after thermal annealing at 120 °C. (a and d) 10 mg mL^{-1}, (b and e) 10^{-1} mg mL^{-1} and (c and f) 10^{-3} mg mL^{-1} in toluene.

© 2025 The Author(s). Published by the Royal Society of Chemistry

Open Access Article. Published on 25 August 2025. Downloaded on 6/15/2026 6:01:51 AM. This article is licensed under a Creative Commons Attribution-NonCommercial 3.0 Unported Licence.

assembly between **3CzPCH** and ***R*/*S*-D** can form highly regular helical nanofibers under annealing treatment, thereby enhancing the CPL signals with large g_{lum} values.

CP-EL properties

Solution-processed CP-OLEDs using these chiral co-assembled films as the EMLs were fabricated to investigate the CP-EL properties, with the following device structure: indium tin oxide (ITO)/PEDOT:PSS (25 nm)/EML (40 nm)/TPBi (35 nm)/Ca (10 nm)/Ag (100 nm). Therein, PEDOT:PSS (poly(2,3-dihydrothieno-1,4-dioxin)-poly(styrenesulfonate)), TPBi (1,3,5-tris(*N*-phenylbenz-imidazole-2-yl)-benzene) and Ca were used as the hole-injection layer, electron-transporting layer and electron-injecting layer, respectively. The devices were defined as *R*/*S*-Cz using **3CzPCH** + 3 wt% ***R*/*S*-D** as the EMLs. The energy level of the devices, chemical structures of the functional materials, EL spectra, a CIE 1931 chromaticity diagram, current density–voltage–luminance (*J*–*V*–*L*) curves, current efficiency–luminance (CE-*L*) curves, CP-EL spectra, and the g_{EL} curves are shown in Fig. 5 and Table 1. *R*/*S*-Cz exhibited intense deep-blue EL emissions at 440 nm, with the CIE coordinates of (0.15, 0.07). These devices exhibited turn-on voltages (V_{on}) of 4.9/5.0 V, maximum luminances (L_{max}) of 3554/3838 cd m^{-2}, maximum current efficiencies (CE_{max}) of 1.41/1.43 cd A^{-1} and maximum external quantum efficiency (EQE_{max}) of 2.38/2.42%.

Notably, ultrastrong CP-EL signals of *R*/*S*-Cz were detected, with g_{EL} values up to −0.47/+0.46 at the corresponding EL peak. It should be noted that the g_{EL} is larger than g_{lum} for the same chiral co-assembled films. Since LC molecules typically reorient under an applied electric field, we characterized the POM images of **3CzPCH**+***R*-D** under applied voltages (0–30 V). The textures of POM images revealed no significant changes even when heated to 140 °C (Fig. S12). Additionally, the CPL signals of the chiral co-assembled films under different voltages were also collected (Fig. S13). The results show that the g_{lum} values remain virtually unchanged, indicating that the applied voltages exert no significant impact on the LC arrangements and the CPL signals. This is attributed to the high viscosity of **3CzPCH**, which suppressed its responsiveness to electric fields. Moreover, the g_{EL} values of *R*/*S*-Cz exhibited minor variations under varying operating voltages (6–9 V) (Fig. S14). Consequently, this anomalous amplification of CP-EL signals is voltage-independent. We propose that this may arise from an additional CP-EL amplification mechanism occurring in the carrier migration process, which needs further investigation.

To comprehensively evaluate the CP-EL performance by simultaneously considering polarization degree and efficiency,

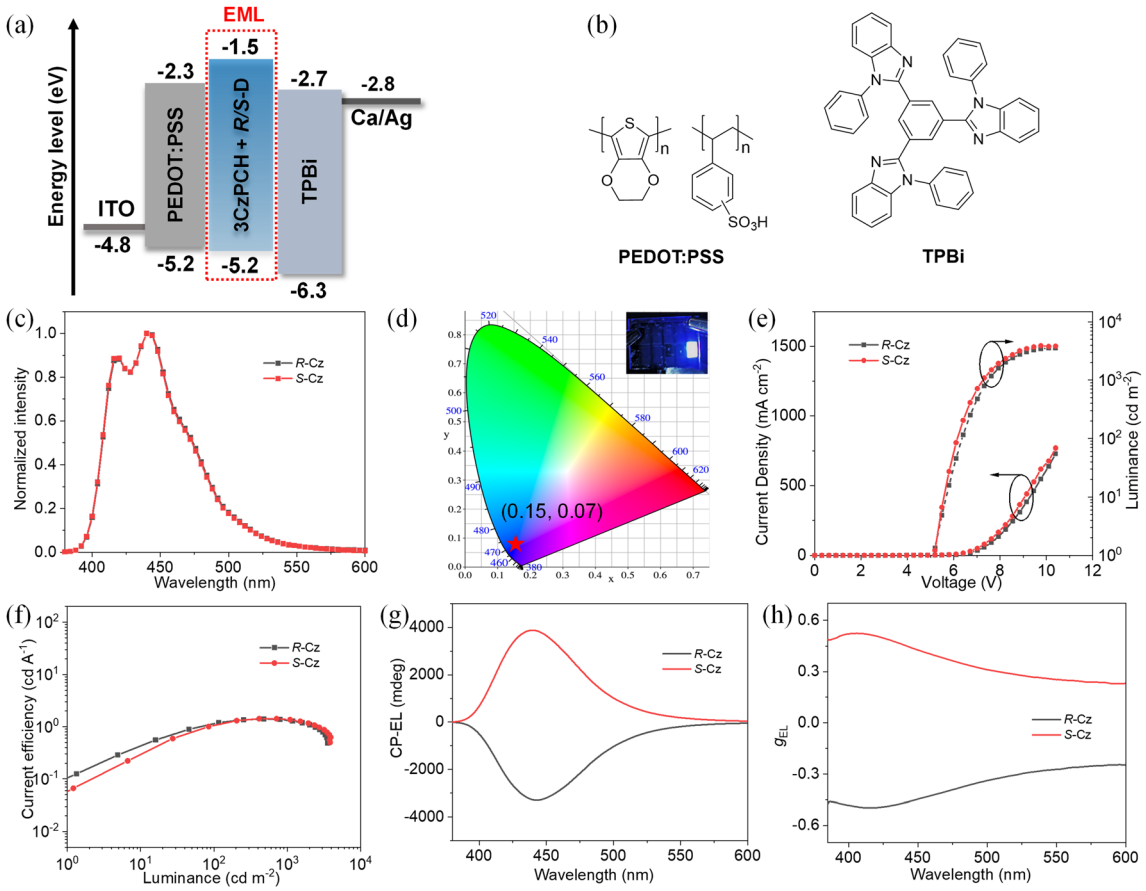

Fig. 5 (a) The energy level diagram of the related materials; (b) chemical structures of functional layer molecules; (c) EL spectra of the *R*/*S*-Cz; (d) CIE 1931 chromaticity diagram; (e) *J*–*V*–*L* characteristics; (f) CE–*L* curves; (g) CP-EL spectra and (h) g_{EL} curves of the *R*/*S*-Cz.

Open Access Article. Published on 25 August 2025. Downloaded on 6/15/2026 6:01:51 AM. This article is licensed under a Creative Commons Attribution-NonCommercial 3.0 Unported Licence.

Table 1 Key device performance data of CP-OLEDs

Device	V_{on}[a] [V]	CE_{max} [cd A^{-1}]	L_{max} [cd m^{-2}]	EQE_{max} [%]	λ_{EL} [nm]	g_{EL}[b]	CIE (x, y)	Q-factor[c] [$\times 10^{-2}$]
R-Cz	4.9	1.41	3554	2.38	440	−0.47	(0.15, 0.07)	1.12
S-Cz	5.0	1.43	3838	2.42	440	+0.46	(0.15, 0.07)	1.11

[a] Recorded at 1 cd m^{-2}. [b] Measured at λ_{EL} = 440 nm. [c] Calculated by EQE × $|g_{EL}|$.

we employ the Q-factor (defined as EQE × $|g_{EL}|$) introduced by Chen *et al.*[57] Accordingly, the Q-factor of *R*/*S*-Cz is calculated to be 1.12/1.11 × 10^{-2}, which represents one of the highest values among the reported CP-OLEDs (Table S3). These results demonstrate an effective strategy for achieving high CP-EL performance through chiral co-assembly of LC-functionalized conductive molecules. More importantly, we show that intense CP-EL signals can be achieved solely *via* the modification of mesogenic units on a carbazole derivative. This LC-functionalization strategy is potentially extensible to other π-conjugated systems, thereby enabling the development of non-doped CP-OLEDs based on LC materials beyond conventional fluorene derivatives.

Conclusions

In summary, an LC-functionalized carbazole derivative, **3CzPCH**, was synthesized by conjugating three carbazole units with two mesogenic units, showing a nematic LC phase. By doping with chiral inducers ***R*/*S*-D** and thermal annealing treatment, the chiral co-assembled films could exhibit strong CPL signals with $|g_{lum}|$ values up to 0.13. In contrast, **3CzPh** without mesogenic units exhibited no LC behaviors. It only had weak chiroptical signals when doped with chiral inducers, due to the absence of chiral co-assembly processes. The formation of orderly helical nanofibers in chiral co-assemblies is crucial for the strong CPL signals. Most importantly, these chiral co-assembled films were successfully employed as the EMLs of solution-processed non-doped CP-OLEDs. These devices achieved ultrastrong CP-EL signals with g_{EL} values of −0.47/+0.46 and a high Q-factor of 1.12 × 10^{-2}, representing one of the highest performances among the reported CP-OLEDs. This work develops an effective strategy for realizing excellent CP-EL performance by using chiral co-assembled EMLs based on LC-functionalized π-conjugated moieties.

Author contributions

H. Li: formal analysis, investigation, methodology, writing – original draft; D. Li: formal analysis, investigation, methodology; Z. Jiang: investigation; Y. Wang: formal analysis, investigation; Y. Cheng: conceptualization, funding acquisition, supervision, writing – review and editing.

Conflicts of interest

There are no conflicts to declare.

Data availability

The data supporting this article have been included as part of the SI. Supplementary information: materials and measurements, experimental details, spectral data and additional data. See DOI: https://doi.org/10.1039/d5sc05196g.

Acknowledgements

This work was supported by the National Natural Science Foundation of China (92156014, 52373188).

References

1 X. Zhan, F.-F. Xu, Z. Zhou, Y. Yan, J. Yao and Y. S. Zhao, *Adv. Mater.*, 2021, **33**, 2104418.
2 M. Zhang, Q. Guo, Z. Li, Y. Zhou, S. Zhao, Z. Tong, Y. Wang, G. Li, S. Jin, M. Zhu, T. Zhuang and S.-H. Yu, *Sci. Adv.*, 2023, **9**, eadi9944.
3 F. Furlan, J. M. Moreno-Naranjo, N. Gasparini, S. Feldmann, J. Wade and M. J. Fuchter, *Nat. Photon.*, 2024, **18**, 658–668.
4 Z.-L. Gong, X. Zhu, Z. Zhou, S.-W. Zhang, D. Yang, B. Zhao, Y.-P. Zhang, J. Deng, Y. Cheng, Y.-X. Zheng, S.-Q. Zang, H. Kuang, P. Duan, M. Yuan, C.-F. Chen, Y. S. Zhao, Y.-W. Zhong, B. Z. Tang and M. Liu, *Sci. China: Chem.*, 2021, **64**, 2060–2104.
5 D.-W. Zhang, M. Li and C.-F. Chen, *Chem. Soc. Rev.*, 2020, **49**, 1331–1343.
6 D. Thakur and S. Vaidyanathan, *J. Mater. Chem. C*, 2025, **13**, 9410–9452.
7 J.-M. Teng, D.-W. Zhang, Y.-F. Wang and C.-F. Chen, *ACS Appl. Mater. Interfaces*, 2022, **14**, 1578–1586.
8 E. Peeters, M. P. T. Christiaans, R. A. J. Janssen, H. F. M. Schoo, H. P. J. M. Dekkers and E. W. Meijer, *J. Am. Chem. Soc.*, 1997, **119**, 9909–9910.
9 Y.-F. Wang, M. Li, J.-M. Teng, H.-Y. Zhou, W.-L. Zhao and C.-F. Chen, *Angew. Chem., Int. Ed.*, 2021, **60**, 23619–23624.
10 L. Frédéric, A. Desmarchelier, L. Favereau and G. Pieters, *Adv. Funct. Mater.*, 2021, **31**, 2010281.
11 A. G. Bispo-Jr, N. A. Oliveira, I. M. S. Diogenis and F. A. Sigoli, *Coord. Chem. Rev.*, 2025, **523**, 216279.
12 J. R. Brandt, X. Wang, Y. Yang, A. J. Campbell and M. J. Fuchter, *J. Am. Chem. Soc.*, 2016, **138**, 9743–9746.
13 T. Huang, L. Yuan, X. Lu, Y. Qu, C. Qu, Y. Xu, Y.-X. Zheng and Y. Wang, *Chem. Sci.*, 2024, **15**, 15170–15177.

© 2025 The Author(s). Published by the Royal Society of Chemistry

Open Access Article. Published on 25 August 2025. Downloaded on 6/15/2026 6:01:51 AM. This article is licensed under a Creative Commons Attribution-NonCommercial 3.0 Unported Licence.

14 S.-Y. Yang, Y.-K. Wang, C.-C. Peng, Z.-G. Wu, S. Yuan, Y.-J. Yu, H. Li, T.-T. Wang, H.-C. Li, Y.-X. Zheng, Z.-Q. Jiang and L.-S. Liao, *J. Am. Chem. Soc.*, 2020, **142**, 17756–17765.
15 J. Kumar, T. Nakashima and T. Kawai, *J. Phys. Chem. Lett.*, 2015, **6**, 3445.
16 Y. Zhang, W. Yu, H. Li, W. Zheng and Y. Cheng, *Chem.–Eur. J.*, 2023, **29**, e202204039.
17 Y. Wang, K. Wan, F. Pan, X. Zhu, Y. Jiang, H. Wang, Y. Chen, X. Shi and M. Liu, *Angew. Chem., Int. Ed.*, 2021, **60**, 16615–16621.
18 H. Zhang, J. Han, X. Jin and P. Duan, *Angew. Chem., Int. Ed.*, 2021, **60**, 4575–4580.
19 Q. Cheng, A. Hao and P. Xing, *ACS Nano*, 2022, **16**, 6825–6834.
20 R. Zhang, J. Gao, N. Li, C. Gao, C. Zhang, H. Wang, F. Sun and T. Yang, *Small*, 2025, **21**, 2409541.
21 Y. Yang, R. C. Da Costa, D.-M. Smilgies, A. J. Campbell and M. J. Fuchter, *Adv. Mater.*, 2013, **25**, 2624–2628.
22 L. Wan, J. Wade, F. Salerno, O. Arteaga, B. Laidlaw, X. Wang, T. Penfold, M. J. Fuchter and A. J. Campbell, *ACS Nano*, 2019, **13**, 8099–8105.
23 J. M. Moreno-Naranjo, F. Furlan, J. Wang, S. T. J. Ryan, T. Matulaitis, Z. Xu, Q. Zhang, L. Minion, M. Di Girolamo, T. Jávorfi, G. Siligardi, J. Wade, N. Gasparini, E. Zysman-Colman and M. J. Fuchter, *Adv. Mater.*, 2024, **36**, 2402194.
24 K.-K. Tan, W.-C. Guo, W.-L. Zhao, M. Li and C.-F. Chen, *Angew. Chem., Int. Ed.*, 2024, **63**, e202412283.
25 C.-H. Guo, Y. Zhang, W.-L. Zhao, K.-K. Tan, L. Feng, L. Duan, C.-F. Chen and M. Li, *Adv. Mater.*, 2024, **36**, 2406550.
26 M. Wang, K. Yang, X. Wang, Z. Tan, K. Pan, J. Deng and B. Zhao, *Adv. Opt. Mater.*, 2024, **12**, 2301513.
27 D. Li, Z. Jiang, S. Zheng, C. Fu, P. Wang and Y. Cheng, *J. Colloid Interface Sci.*, 2025, **678**, 1213–1222.
28 Y. He, S. Lin, J. Guo and Q. Li, *Aggregate*, 2021, **2**, e141.
29 K. Akagi, *Bull. Chem. Soc. Jpn.*, 2019, **92**, 1509–1655.
30 X. Zhang, Y. Xu, C. Valenzuela, X. Zhang, L. Wang, W. Feng and Q. Li, *Light: Sci. Appl.*, 2022, **11**, 223.
31 Y. Feng, G. Gao, X. Wen, Z. Chen, J. Huang, C. Yang, X.-F. Jiang, L. Polavarapu, G. Zhou and X. Hu, *Adv. Funct. Mater.*, 2025, **35**, 2421338.
32 K. Horie, Y. Fujita, K. Kaneko, T. Hanasaki and K. Akagi, *ACS Appl. Mater. Interfaces*, 2025, **17**, 15988–15999.
33 Z. Li, R. Lan, J. Bao, W. Hu, M. Wang, L. Zhang and H. Yang, *ACS Appl. Mater. Interfaces*, 2022, **14**, 8490–8498.
34 S. Yoshida, S. Morikawa, K. Ueda, K. Kaneko, T. Hanasaki and K. Akagi, *ACS Appl. Mater. Interfaces*, 2024, **16**, 3991–4002.
35 J. Yuan, X. He, L. Chen, X. Lu and Q. Lu, *Angew. Chem., Int. Ed.*, 2025, **64**, e202419924.
36 D. Di Nuzzo, C. Kulkarni, B. Zhao, E. Smolinsky, F. Tassinari, S. C. J. Meskers, R. Naaman, E. W. Meijer and R. H. Friend, *ACS Nano*, 2017, **11**, 12713–12722.
37 M. Oda, H.-G. Nothofer, G. Lieser, U. Scherf, S. C. J. Meskers and D. Neher, *Adv. Mater.*, 2000, **12**, 362–365.
38 C. Kulkarni, M. H. C. van Son, D. Di Nuzzo, S. C. J. Meskers, A. R. A. Palmans and E. W. Meijer, *Chem. Mater.*, 2019, **31**, 6633–6641.
39 D.-M. Lee, G.-E. Kim, J.-H. Kim and C.-J. Yu, *J. Mater. Chem. C*, 2023, **11**, 3300–3305.
40 D.-M. Lee, J.-W. Song, Y.-J. Lee, C.-J. Yu and J.-H. Kim, *Adv. Mater.*, 2017, **29**, 1700907.
41 C.-J. Yu, D.-M. Lee, J.-K. Han, Y.-J. Lee, S.-W. Kim, E.-J. Choi and J.-H. Kim, *Adv. Opt. Mater.*, 2022, **10**, 2101674.
42 S. Umadevi, X. Feng and T. Hegmann, *Adv. Funct. Mater.*, 2013, **23**, 1393–1403.
43 L. Zhang, K. Zhao, H. Li, T. Zhang, D. Liu and Y. Han, *J. Polym. Sci., Part B: Polym. Phys.*, 2019, **57**, 1572–1591.
44 Z. Hu, G. Wang, S. Zhao, S. Jiang, J. Hu and A. Reheman, *J. Mol. Liq.*, 2023, **369**, 120891.
45 G. Qian, X. Yang, X. Wang, J. D. Herod, D. W. Bruce, S. Wang, W. Zhu, P. Duan and Y. Wang, *Adv. Opt. Mater.*, 2020, **8**, 2000775.
46 B. He, Q. Zhong, Q. Dong, X. Yang, S. J. Cowling, W. Qiao, D. W. Bruce, W. Zhu, P. Duan and Y. Wang, *Mater. Horiz.*, 2024, **11**, 1251–1260.
47 X. Lai, Q. Zhong, C. Xiao, S. J. Cowling, P. Duan, D. W. Bruce, W. Zhu and Y. Wang, *Chem. Commun.*, 2024, **60**, 2026–2029.
48 G. Zou, Z. Jiang, D. Li, Q. Li and Y. Cheng, *Chem. Sci.*, 2024, **15**, 18534–18542.
49 H. Li, D. Li, C. Fu, Y. Chen and Y. Cheng, *Adv. Opt. Mater.*, 2025, **13**, 2402426.
50 S. Oner and M. R. Bryce, *Mater. Chem. Front.*, 2023, **7**, 4304–4338.
51 B. Wex and B. R. Kaafarani, *J. Mater. Chem. C*, 2017, **5**, 8622–8653.
52 Y. Liu, S. Xu, J. Li, Y. Xin, G. Zhao, B. Ye and S. Cao, *Polym. Adv. Technol.*, 2008, **19**, 793–800.
53 B. Ruhstaller, J. C. Scott, P. J. Brock, U. Scherf and S. A. Carter, *Chem. Phys. Lett.*, 2000, **317**, 238–244.
54 H. Wu, Z. Chen, W. Chi, A. K. Bindra, L. Gu, C. Qian, B. Wu, B. Yue, G. Liu, G. Yang, L. Zhu and Y. Zhao, *Angew. Chem., Int. Ed.*, 2019, **58**, 11419–11423.
55 Z. Yang, X. Fan, X. Liu, Y. Chu, Z. Zhang, Y. Hu, H. Lin, J. Qian and J. Hua, *Chem. Commun.*, 2021, **57**, 3099–3102.
56 G. Albano, G. Pescitelli and L. Di Bari, *Chem. Rev.*, 2020, **120**, 10145–10243.
57 W.-C. Guo, W.-L. Zhao, K.-K. Tan, M. Li and C.-F. Chen, *Angew. Chem., Int. Ed.*, 2024, **63**, e202401835.